Ninth International Conference on CFD in the Minerals and Process Industries
CSIRO, Melbourne, Australia
10-12 December 2012

MODELLING THE IMPACT OF TWO DIFFERENT FLOCCULANTS ON THE PERFORMANCE OF A THICKENER FEEDWELL

Michel TANGUAY[1*], Phillip FAWELL[2] and Stephen ADKINS[3]

[1]CSIRO Mathematics, Informatics and Statistics, Clayton, Victoria 3169, AUSTRALIA
[2]CSIRO Process Science and Engineering, Waterford, Western Australia 6152, AUSTRALIA
[3] BASF Performance Products plc, P.O. Box 38, BD12 0JZ, Bradford, UK
*Corresponding author, Email address: michel.tanguay@csiro.au

ABSTRACT

The performance of a thickener feedwell depends not only on its ability to generate large-sized aggregates from feed particles but also on aggregate density. The performance of the flocculant BASF Rheomax® 1050 has been previously compared to a conventional anionic flocculant in pipe reactor experiments, suggesting that the Rheomax product can generate denser aggregates (i.e. larger effective fractal dimension). Such aggregates are generally stronger and reduce the need for solids dilution, with both factors favouring faster settling rate at the feedwell exit. To investigate the impact of the internal aggregate structure on the flocculation performance of a feedwell, Computational Fluid Dynamics (CFD) simulations of a basic open feedwell with shelf design were carried out for both flocculants. A calcite with a fine particle size (Omyacarb 5) was modelled to emphasise the impact of the flocculation process on flow fields at the feedwell exit. Simulations were conducted using CFX-4.4 two-phase flow formulation incorporating equations for a population balance model of the flocculation process. The impact of the fractal dimension on the effectiveness of the aggregation process is presented for low and high solids concentrations. Comparison of the performance of the flocculants is presented in terms of both predicted mean aggregate size and settling flux.

NOMENCLATURE

A control volume face area [m^2]
A_t thickener cross section area [m^2]
C linearised coupling source term coefficient[kg m^{-3} s^{-1}]
$C_{1\varepsilon}$ turbulence parameter
$C_{2\varepsilon}$ turbulence parameter
C_s concentration of flocculant on solid phase
C_l concentration of flocculant in liquid phase
D_f fractal dimension
d_{agg} average aggregate size [m]
d_p average primary particle size [m]
F conditional breakage
G flocculant source term [kg m^{-3} s^{-1}]
$\mathbf{g}$ gravity [m s^{-2}]
H ratio of fractal volume over mass equivalent volume
k turbulence kinetic energy [m^2 s^{-2}]
k_2 population balance model constant [m^{-2}]
k_3 population balance model constant
k_4 population balance model constant [m s^{-1}]
N_i number of particles in bin i per mass of solid [# kg^{-1}]
$\boldsymbol{n}$ control volume face normal [m^2]
P probability density per mass of solid [# kg^{-1} m^{-3}]
P_k turbulence production term [kg m^{-1} s^{-3}]
p pressure [N m^{-2}]
S breakage kernel [s^{-1}]
t time [s]
$\boldsymbol{U}$ velocity vector [m s^{-1}]
$\boldsymbol{x}$ position vector [m]

α solid phase volume fraction
β aggregation kernel [m^3 s^{-1}]
ε turbulence dissipation [m^2 s^{-3}]
ε_o turbulence dissipation normalisation = 1 [m^2 s^{-3}]
σ_k turbulence parameter
σ_ε turbulence parameter
λ_s primary particle surface area per volume [m^{-1}]
ϕ_s volume fraction of solid phase
ϕ_{eff} effective volume fraction of fractal aggregates
Θ flocculant degradation parameter
ρ density [kg m^{-3}]
μ dynamic viscosity [kg m^{-1} s^{-1}]

INTRODUCTION

Hydrometallurgical processing of minerals invariably involves at least one stage of solid-liquid separation, with gravity thickeners typically employed to treat high volumetric throughputs of suspensions. When particle sizes are small (e.g. -80 µm), throughputs are enhanced through application of water-soluble polymers (flocculants) that induce aggregation, thereby accelerating settling rates.

Almost all measured properties of the flocculated system are affected by the open, low density (porous) structures of the aggregates formed. Initial mudline settling rates are well known to be determined by both aggregate size and density. Critically, such aggregate structures influence the effective solids volume fraction (ϕ_{eff}), as shown below (Potanin and Uriev, 1991):

$$\phi_{eff} = \phi_s \left(\frac{d_{agg}}{d_p} \right)^{3-D_f} \quad (1)$$

Where ϕ_s is the solids volume fraction, d_{agg} and d_p are the aggregate and particle diameters, respectively, and D_f the fractal dimension. The value for D_f can strongly affect hindered settling rates and thereby the flocculation response to changes in solids concentration.

In the majority of tailings thickening applications, solids dilution prior to flocculation is required to maximise the settling flux and throughput, with dilution streams being added to the feed slurry before it enters the feedwell. Any flocculant that can produce an aggregate with a higher D_f will potentially reduce the need for dilution.

BASF's Rheomax® series of products are recent commercial flocculants that may provide a change in aggregate structure (Adkins, 2008). Grabsch *et al*. (2012) conducted a detailed study of the flocculation kinetics of Rheomax 1050 and a conventional anionic flocculant (BASF Magnafloc 336) when applied to a fine calcite slurry. They observed a higher optimum solids concentration for flocculation with Rheomax 1050, with calculated settling fluxes at or above that concentration significantly higher than when Magnafloc 336 was used. They then applied a population balance (PB) model derived for polymer bridging flocculation to their kinetic data, with the parameter estimation process indentifying a higher D_f value for Rheomax 1050.

Incorporation of the PB model into the CFD code used to describe feedwell hydrodynamics (PB-CFD) has been used previously to optimise flocculation performance (Nguyen *et al.* (2006)). However, the implications from flocculant selection have never previously been considered. This study utilises the PB parameters generated for the flocculation of calcite with the two flocculants to provide the first PB-CFD study of how achieving a higher aggregate density may influence the predicted feedwell response under different conditions.

MODEL DESCRIPTION

Two-phase flow modelling

In CFX-4.4, multiphase flow is captured using an Eulerian-Eulerian formulation where both phases are treated as separate fluids (with mass and momentum conservation) and connected via a source term to account for the drag between the two phases. The pressure field for each phase is assumed to be identical. The equations for the mass and momentum conservation of each phase are presented in below (see Equation (2)).

$$\begin{aligned}
&\frac{\partial}{\partial t}\left(\phi_s\rho_s\right)+\nabla\cdot\left(\phi_s\rho_s\mathbf{U}_s\right)=0\\
&\frac{\partial}{\partial t}\left(\phi_s\rho_s\mathbf{U}_s\right)+\nabla\cdot\left(\phi_s\rho_s\mathbf{U}_s\mathbf{U}_s\right)\\
&\quad-\nabla\cdot\left(\phi_s\mu_s\left(\nabla\mathbf{U}_s+\left(\nabla\mathbf{U}_s\right)^T\right)\right)\\
&\quad=\phi_s\rho_s\mathbf{g}-\phi_s\nabla p-C\left(\mathbf{U}_s-\mathbf{U}_l\right)\\
&\frac{\partial}{\partial t}\left(\left(1-\phi_s\right)\rho_l\right)+\nabla\cdot\left(\left(1-\phi_s\right)\rho_l\mathbf{U}_l\right)=0\\
&\frac{\partial}{\partial t}\left(\left(1-\phi_s\right)\rho_l\mathbf{U}_l\right)+\nabla\cdot\left(\left(1-\phi_s\right)\rho_l\mathbf{U}_l\mathbf{U}_l\right)\\
&\quad-\nabla\cdot\left(\left(1-\phi_s\right)\mu_l\left(\nabla\mathbf{U}_l+\left(\nabla\mathbf{U}_l\right)^T\right)\right)\\
&\quad=\left(1-\phi_s\right)\rho_l\mathbf{g}-\left(1-\phi_s\right)\nabla p+C\left(\mathbf{U}_s-\mathbf{U}_l\right)
\end{aligned}\tag{2}$$

The above equations are essentially the conservation equations for two compressible substances coupled by a linearised drag term. The coupling source term between the two phases is based on the Stokes drag for a sphere modified by the Richardson and Zaki (1955) correction to account for the hindrance of surrounding particles:

$$C=\frac{18\mu_l^{visc}}{d^2}\phi_{eff}\left(1-\phi_s\right)\left(1-\phi_{eff}\right)^{-3.65}\tag{3}$$

The effective laminar viscosity term used in model of the liquid phase is adjusted to account for the presence of the solid phase. As the solid volume fraction increases, the interactions between the solid and liquid phase become more effective at dissipating momentum. In the present model, this effect and is represented by adjusting the molecular viscosity using a correction proposed by Govier and Aziz (1972) (see Equation (4)). Note that for the range of solid fractions considered in this study, the viscosity correction is less than a factor of 2.

$$\mu_l^{visc}=\frac{\mu_l^{\text{single phase}}}{\left(1-\phi_{eff}/0.65\right)^2}\tag{4}$$

Turbulence model

In the present work, a standard k-ε model was used to represent the turbulence within the liquid phase, while the solid phase was assumed laminar. Wall functions were applied at all solid walls.

$$\begin{aligned}
&\frac{\partial}{\partial t}\left(\left(1-\phi_s\right)\rho_l k\right)+\nabla\cdot\left(\left(1-\phi_s\right)\rho_l\mathbf{U}_l k\right)=\\
&\quad\nabla\cdot\left(\left(\mu_l^{visc}+\frac{\mu_l^{turb}}{\sigma_k}\right)\nabla k\right)+\left(1-\phi_s\right)\left(P_k-\rho_l\varepsilon\right)\\
&\frac{\partial}{\partial t}\left(\left(1-\phi_s\right)\rho_l\varepsilon\right)+\nabla\cdot\left(\left(1-\phi_s\right)\rho_l\mathbf{U}_l\varepsilon\right)=\\
&\quad\nabla\cdot\left(\left(\mu_l^{visc}+\frac{\mu_l^{turb}}{\sigma_\varepsilon}\right)\nabla\varepsilon\right)\\
&\quad+\left(1-\phi_s\right)\left(\frac{\varepsilon}{k}\right)\left[C_{1\varepsilon}P_k-C_{2\varepsilon}\rho_l\varepsilon\right]\left(P_k-\rho_l\varepsilon\right)\\
&P_k\equiv\mu_l\nabla\mathbf{U}_l\cdot\left(\nabla\mathbf{U}_l+\left(\nabla\mathbf{U}_l\right)^T\right)-\frac{2}{3}\nabla\mathbf{U}_l\cdot\left(\mu_l\nabla\mathbf{U}_l+\rho_l k\right)
\end{aligned}\tag{5}$$

Flocculant and population balance modelling

The population balance for aggregation used here is similar to the model developed in Heath and Koh (2003), Heath *et al.* (2006) and Nguyen *et al.* (2006). A summary of the relevant governing equations is presented below.

$$\begin{aligned}
&\phi_s\rho_s\frac{D}{Dt}\left(P\left(d,\mathbf{x},t\right)\right)-\nabla\cdot\left(\Gamma\nabla P\left(d,\mathbf{x},t\right)\right)=\phi_s\rho_s S_P\\
&S_P\equiv\frac{1}{2}\int_0^d\beta\left(d-y,y\right)P\left(d-y,\mathbf{x},t\right)P\left(y,\mathbf{x},t\right)dy\\
&\quad-P\left(d,\mathbf{x},t\right)\int_0^d\beta\left(d,y\right)P\left(y,\mathbf{x},t\right)dy\\
&\quad+\int_d^\infty S\left(y\right)F\left(d\mid y\right)P\left(y,\mathbf{x},t\right)dy-S\left(d\right)P\left(d,\mathbf{x},t\right)dy
\end{aligned}\tag{6}$$

The aggregation kernel used in this study is the collision kernel developed by Saffman and Turner (1956) where:

$$\beta\left(x,y\right)\equiv1.294\cdot0.5\cdot\left(\frac{C_s}{C_s^{\max}}\right)\sqrt{\frac{\rho_l\varepsilon}{\mu_l}}\left(x+y\right)^3\tag{7}$$

The breakage kernel is set to be inversely proportional to the adsorbed flocculant concentration and follows from the work of Heath and Koh (2003), Heath *et al.* (2006):

$$S\left(x\right)\equiv0.5\frac{k_2\left(\varepsilon/\varepsilon_o\right)^{k_3}\mu_l^{visc}x}{\left(1-\Theta\right)\left(C_s\rho_s/\lambda_s\right)}\tag{8}$$

Following the previous works, aggregates are assumed to break up in half. Therefore, the particle size distribution generated by the breakup of an aggregate of a certain size *d* is represented by:

$$F\left(d\mid y\right)\equiv\delta\left(2d-y\right)\tag{9}$$

At any given location, the particle size population is discretised using geometrically increasing size interval following the approach described in Batterham *et al*. (1981) and Hounslow *et al.* (1988).

$$
\begin{aligned}
&N_i \equiv \int_{d_i^3}^{d_{i+1}^3} P(y,\mathbf{x},t)\,dy \\
&d_i^3 \equiv 2^i d_o^3 \\
&\phi_s\rho_s \frac{D}{Dt}\left(N_i(\mathbf{x},t)\right) - \nabla\cdot\left(\Gamma\nabla N_i(\mathbf{x},t)\right) = \phi_s\rho_s\dot{N}_i \\
&\dot{N}_i \equiv \left[\sum_{j=1}^{i-2} 2^{j-i+1}\beta_{i-1,j}N_{i-1}N_j + \frac{1}{2}\beta_{i-1,i-1}N_{i-1}N_{i-1}\right. \\
&\qquad \left. -\sum_{j=1}^{i-1} 2^{j-i}\beta_{i,j}N_iN_j - \sum_{j=i}^{\infty}\beta_{i,j}N_iN_j\right]\phi_s\rho_s \\
&\qquad - S_iN_i + 2S_{i+1}N_{i+1}
\end{aligned}
\tag{10}
$$

The presence of the flocculant is accounted for in both phases and the propagation model follows from the work of Nguyen *et al.* (2006), Heath and Koh (2003) and Heath *et al.* (2006).

$$
\begin{aligned}
&\frac{\partial}{\partial t}\left(\phi_s\rho_sC_s\right) + \nabla\cdot\left(\phi_s\rho_s\mathbf{U}_sC_s\right) = G \\
&\frac{\partial}{\partial t}\left(\left(1-\phi_s\right)\rho_lC_l\right) + \nabla\cdot\left(\left(1-\phi_s\right)\rho_l\mathbf{U}_lC_l\right) = -G \\
&G \equiv 1.294\cdot(0.1)\cdot\sqrt{\frac{\rho_l\varepsilon}{\mu_l}}C_l\left(1-\phi_s\right)\rho_l\left(\frac{C_s^{\max}-C_s}{C_s^{\max}}\right)\phi_sK
\end{aligned}
\tag{11}
$$

$$
K \equiv \frac{\text{fractal volume}}{\text{equ. mass volume}} = \frac{\sum_i \left(d_i/d_p\right)^{\frac{9}{D_f}} N_i}{\sum_i \left(d_i/d_p\right)^3 N_i}
$$

With an increasing number of collisions, the flocculant losses its ability to form stable aggregates. This is captured by a flocculant degradation parameter computed using Equation (12).

$$
\begin{aligned}
&\frac{\partial}{\partial t}\left(\phi_s\rho_s\Theta\right) + \nabla\cdot\left(\phi_s\rho_s\mathbf{U}_s\Theta\right) = \\
&\qquad \phi_s\rho_sk_4\varepsilon^{k_3}\mu\phi_{ref}\left(\frac{C_s}{C_{s_{MAX}}}\right)\left[1-\Theta\left(\frac{\phi_s}{\phi_{ref}}\right)^{1/3}\right]
\end{aligned}
\tag{12}
$$

Notable differences between the formulation presented above and that of Heath *et al.* (2006) pertain to the definition and use of a mixing index. In the present work, the ratio of adsorbed flocculant over the saturation value is used as a representation of how well mixed is the system. Additionally, the aggregation and breakage kernels presented in this work can be obtained through multiplying those found in Heath *et al.* (2006) by the adsorbed flocculant saturation ratio (or mixing index). This approach has the benefit of making the aggregation kernel proportional to the flocculant adsorbed thus preventing aggregation before the slurry can interact with the flocculant.

Computational domain and simulation conditions

The computational domain used was a 20 m diameter thickener with a 4 m diameter open feedwell fitted with a 0.4 m wide shelf. Flocculant is injected from a sparge located in the middle of the shelf, 45^o away from the inlet. Additional details of the domain and boundary conditions labels are found in Figure 1. The thickener's size and shape are based on common designs in the industry and the domain used in previous studies (Nguyen *et al.*, 2012). The domain was meshed using a multiblock structured grid with 166K elements and 212K nodes. The perimeter of the axisymmetric grid was discretised with 64 elements and the feedwell comprised of 65K elements (note that the grid dimensions also followed from Nguyen *et al.*, 2012).

The inlet boundary was set to be a fixed velocity condition (same velocity for both phases) with the direction specified to be nearly tangential to the feedwell. The overflow boundary was set to a fixed outflow velocity normal to the surface but with a zero velocity for the solid phase. Note that in the numerical solutions the solid concentration at the overflow is essentially zero thus validating the zero velocity boundary conditions. Attempts to specify a non-zero velocity for the solid phase have resulted in convergence problems.The underflow was set to be a free mass outflow boundary where the mass flux is set such as to satisfy the mass balance in the domain. Flocculant was injected through a small inlet at a prescribe velocity and a solid phase volume fraction of zero; its concentration was set to 0.01% at the sparge and the velocity of the liquid was adjusted for each case such as to have 20 g of flocculant per tonne of solids, representing a typical dosage.

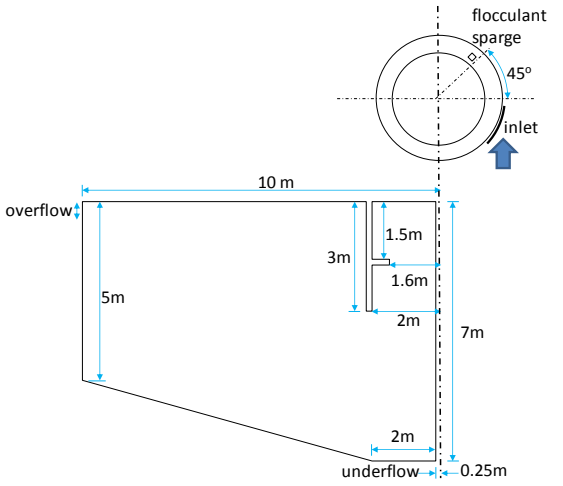

Figure 1: Dimensions of computational domain.

The particle size distribution used was based on a measured sample of Omayacarb 5 calcite (Omya Australia Pty Ltd.) with a mean mass weighted size of 5 microns. The probability density function for the particle size is presented in Figure 2.

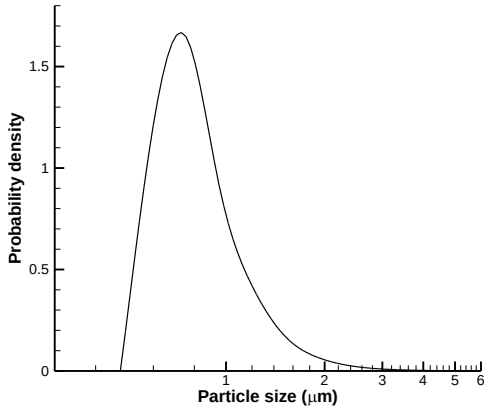

Figure 2: Probability density function of the particle size for Omyacarb 5.

The parameters for the interaction between the flocculant and the calcite particles were determined from a

flocculation kinetics study conducted on a pipe reactor (Grabsch *et al*. (2012)) and are shown below in Table 1.

Parameter	Magnafloc 336	Rheomax 1050
k_2 (dosage)	96.7	90.9
k_3 (shear)	0.70	0.70
k_4 (irreversibility)	405	470
D_f (fractal dimension)	2.40	2.55

Table 1: Parameter for the population balance model for Omyacarb 5 calcite flocculation.

Post-processing and particle tracking

To provide additional insight into the performance of the feedwell as a continuous reactor, particle paths were extracted in post-processing. Standard approaches for the calculation of streamlines involve interpolation of the control-volume velocities (located at the cell centres). However, using streamlines to collect data was less than successful in the present case due to the large fraction of streamlines terminating prematurely and many regions of the domain were not covered. The apparent discrepancy between the transport of particles following streamlines and the computed mass transport of the solid phase is due to differences between the cell centred velocity (also referred to as the advected velocity) and the face centred velocity used to compute the control-volume fluxes (also referred to as the advecting velocity). The difference between the two velocity fields is typically a function of the mesh size and local flow gradients.

A flux based scheme was considered in an effort to mitigate this resolution effect on the calculation of particle path and to reconcile with the distribution obtained from an Eulerian scalar transport equation. The objective was to capture the Eulerian-based flux but with the Lagrangian particle tracking. In order to relate the transport of a particle within a control volume to the fluxes at the faces, one would need to know the internal routing of the streamlines. At the lowest level of approximation, one could assume that all particles within the control volume are well mixed and then distribute at the out-going faces based on the local flux. This approach is very similar to the earlier work of Smith and Schwartz (1983, 1984) on fluid transport in fractured media. Under the well mixed approximation, a particle has a probability of leaving through a given face of a volume proportional to the fraction of the fluid flowing through it. This guarantees that the number of particles passing through any given face is consistent with the flux computed in the Eulerian scheme. The probability of a particle leaving through the i^{th} face of a control volume is:

$$\text{prob } face_i = \frac{max\left[0,\left(A\boldsymbol{U}\cdot\boldsymbol{n}\right)_i\right]}{\sum_{j=1}^{\text{all faces}} max\left[0,\left(A\boldsymbol{U}\cdot\boldsymbol{n}\right)_j\right]} \qquad (13)$$

Once the exit face is determined, the exit location for the particle is determined randomly with a uniform probability distribution. Equation (14) is used for the calculation of the residence time of a particle within a cell. In this equation, the velocity is the current cell centre velocity.

$$\Delta t = \frac{\boldsymbol{U}\cdot\boldsymbol{x}}{\boldsymbol{U}\cdot\boldsymbol{U}} \qquad (14)$$

A comparison between the random walk and streamline approach was performed for one of the test cases considered in this work (Rheomax 1050, 5% w/w solids inlet). Figure 4 presents a side-by-side comparison between the particle locations computed using the present random walk scheme and those following streamlines based on control-volume velocity field. The random walk approach exhibit significantly more diffusion than the streamlines suggests. This illustrates the limitations of the streamlines where the average cell velocity for the solid phase does not accurately represent the mass transport. The mean height as a function of time is presented in Figure 3. The comparisons show that both approaches yield very similar mean values but with a slightly larger standard deviation for the random walk approach.

The proposed approach offers significant benefits in terms of conservation of number of particles as well as provides better representation of the actual solid distribution as determined by the Eulerian-Eulerian simulation. However, the well-mixed approximation used in the present work can lead to excessive diffusion of the particles within the domain. While the average may provide a good representation of the data, the variance estimates may be larger warranted. Further work in this path will consider more sophisticated approaches such as Hull and Koslow (1986), Berkowitz *et al.* (1994) and Rhodes and Blunt (2006) where the well-mixed approximation is replaced by a more detailed sub-grid flow distribution.

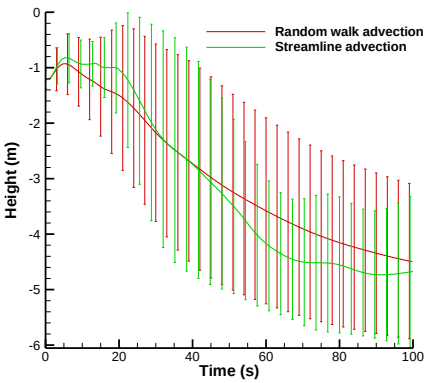

Figure 3: Comparison of average height of particle as a function of time between randow walk and streamline advection scheme.

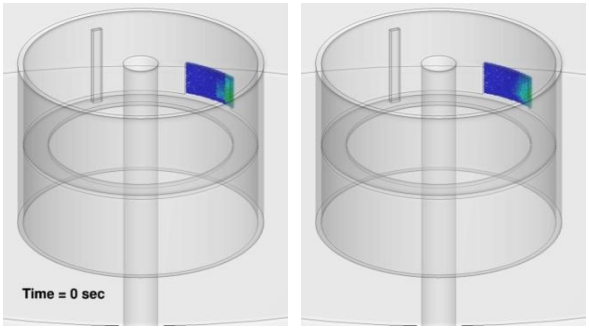

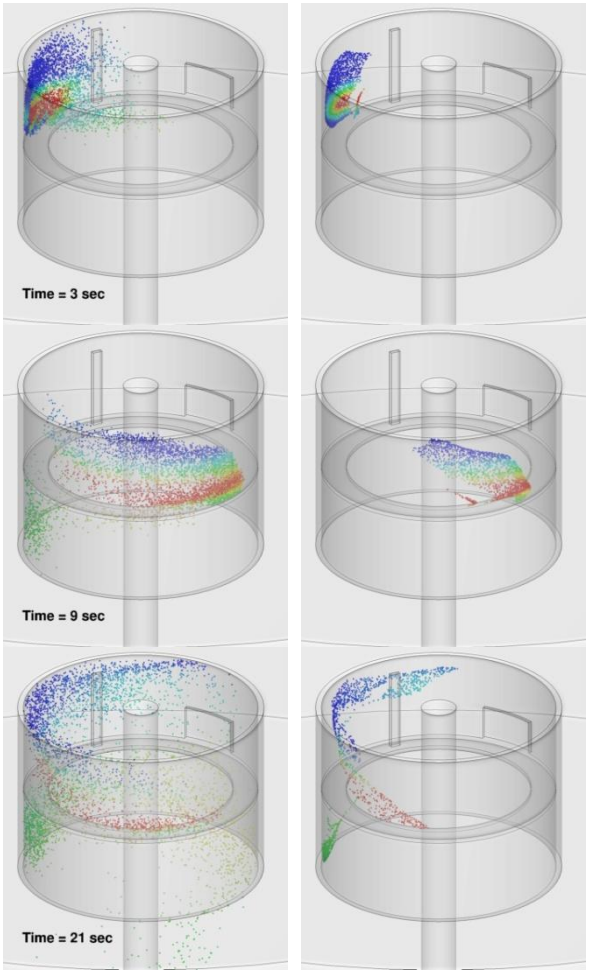

Random walk advection Streamline advection

Figure 4: Side-by-side comparison of particle locations in the feedwell as a function of time between random walk and streamline advection.

RESULTS

Simulations comparing Magnafloc 336 and Rheomax 1050 performance were conducted in tandem over a range of slurry concentrations. The simulation flow parameters are presented in Table 2. Results were post-processed to extract 50000 particle paths initiated at the inlet. The particles were advanced using a random walk approach discussed in the previous section. The large number of paths provided a statistical representation of the flow history through the thickener and was determined by progressively increasing the number of paths until the results were unchanged. Variations in the results were quantified by computing the standard deviation from the sample set and are presented alongside the average.

Inlet flow rate	1000 m^3/h
Inlet velocity	1.5 and 2.4 m/s
Solid concentration at inlet	5,10,15 and 20% w/w
Flocculant injection at sparge	20g/tonne solid
Flocculant concentration at sparge	0.01%
Overflow rate	155, 152, 148, 145 m^3/h

Table 2: Flow conditions for simulations.

In an effort to assess the impact of shear rate on the feedwell flocculation performance, two different inlet flow velocities were tested while keeping the overall flow rate fixed (inlet size was decreased accordingly). Baseline tests were conducted at a velocity of 1.5 m/s which is regarded as optimal for many thickeners. The higher velocity was set to 2.4 m/s, which is near the maximum recommended velocity for most industrial applications. Comparison of the average aggregate size leaving the feedwell (see Figure 5) shows that for both flocculants, the overall size decreases for all solid fractions at the higher flow rate. This result can be explained by the higher shear experienced by the particles as they travel over the shelf. Using the particle path post-processing, the shear rate experience as a function of time in the feedwell can be shown to be significantly higher for the high speed injection (see Figure 6). It is interesting to note from Figure 5 that the decrease in aggregate size is essentially independent on the choice of flocculant.

Earlier experimental work of Grabsch *et al*. (2012) showed that the optimum solids concentration for aggregation using Rheomax was higher than for Magnafloc. Feedwell modelling indicates a similar trend with Rheomax producing the largest mean aggregate size at a solid fraction of 10% w/w while Magnafloc peak size was at or below a solid fraction of 5% w/w (see Figure 5). It is interesting to note that the inlet velocity does not appear to significantly impact the optimal mass fractions.

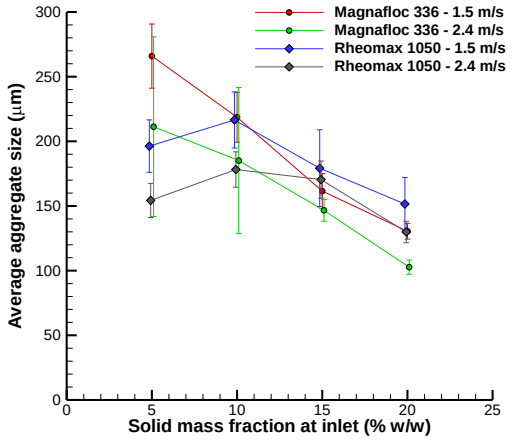

Figure 5: Comparison of average aggregate size at the feedwell exit for Rheomax and Magnafloc. One standard deviation of the fluctuation is shown.

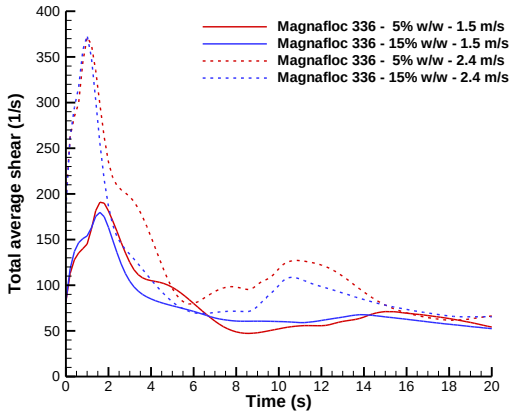

Figure 6: Comparison of total average shear rate as a function of time for low (1.5 m/s) and high (2.4 m/s) velocity and low (5% w/w) and high (15% w/w) solid concentration.

The solid residence time within the feedwell was estimated based on the post-processed particle paths. The average residence time with both flocculant decreases sharply with increased solids concentration as shown in Figure 7. It is also noteworthy that an increase in inlet velocity results in a clear increase in the mean residence time. The increase in the momentum allows the slurry to swirl longer above the shelf thus increasing the residence time. The standard deviation of the sample set was not presented in Figure 7 as it did not provide an appropriate description of the large spread in the residence time. The probability density for the residence time for two Rheomax cases (5 and 15% w/w at 1.5 m/s inlet) is presented in Figure 8. It is interesting to note that the probability density exhibits similar patterns for both cases (large initial peaks followed by long decaying tail). The tail segment of the distribution can be associated with the particles that swirl near the core of the feedwell where as the initial peaks are associated with particles falling off the shelf. Figure 8 suggests that the increase in solid fraction resulted in an increase in the amount of solids spilling over the shelf.

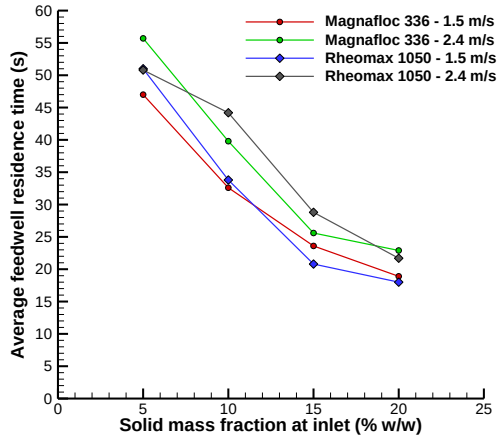

Figure 7: Comparison of average solid residence time in the feedwell for Rheomax and Magnafloc at different solid concentration.

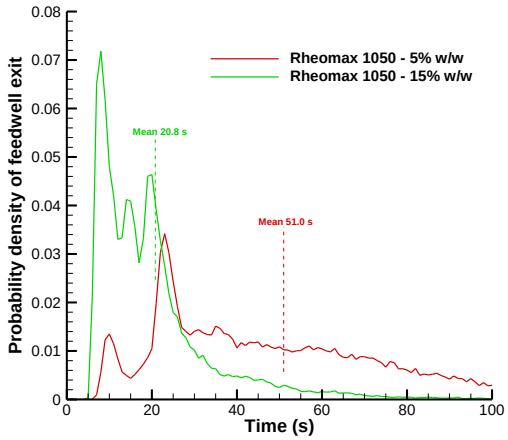

Figure 8: Impact of the injected solid mass fraction on the probability density function of the feedwell residence time for particles undergoing random walk.

The aggregate settling rate is critical for estimating the impact of flocculation on thickener operation since it is one factor possibly limiting throughput. Figure 9 presents the average particle settling velocity for the different cases as a function of time in the thickener. Note that for each curve, the times where the mean particle height passed below the shelf height and the feedwell exit are indicated by a triangle and a circle, respectively. After the solid phase has dropped below the feedwell, the velocity becomes steady until it reaches the sediment bed where it decreases. Since the present study did not include any rheological modelling of the bed, no additional conclusions could be drawn with regards to other limiting factors such as the bed compressibility. However, considering only solid-liquid separation in the fluidised region between the feedwell and the bed, estimates on the theoretical limit of the thickener for extraction of pure solid can be obtained from the phase averaged slip velocity through the thickener cross-section (see Equation (15)). Results for the various cases considered can be found in , where Rheomax is shown to outperform Magnafloc at all solids concentrations. This result is not surprising since Rheomax produced larger aggregates (except at the lowest solid concentration) with higher density due to the higher fractal dimension thus resulting in higher settling velocities (see Figure 9).

$$\text{throughput} \equiv \overline{\phi\left(\mathbf{U}_s - \mathbf{U}_l\right) \cdot A_t} \qquad (15)$$

Injected slurry concentration	Maximum throughput of solids (tonne/h)	
	Rheomax	Magnafloc
5% w/w	167.5	141.2
10% w/w	323.0	181.7
15% w/w	359.4	157.1
20% w/w	348.1	158.6

Table 3: Theoretical maximum throughput of solids based on settling velocity and volume fraction post- feedwell.

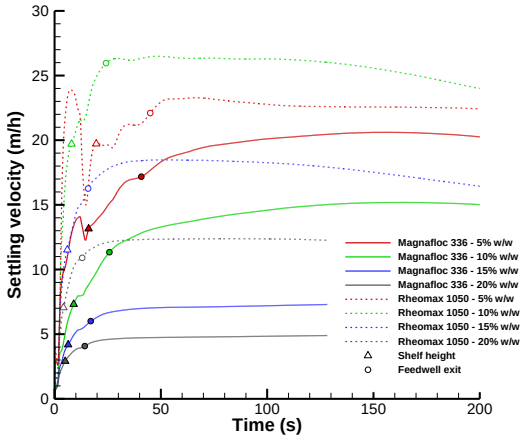

Figure 9: Average settling velocity as a function of the time of flight for different flocculants and concentrations of injected slurry.

CONCLUSION

Multi-phase simulations comparing the performance of Rheomax 1050 and Magnafloc 336 in the context of thickener operation have been conducted. Above 5% w/w solid concentration, Magnafloc results showed a steady downward trend in the size of aggregates produced with

increasing solid concentration. Rheomax results presented a different trend where the mean aggregate size peaked at a solid concentration of 10% w/w. This shift in the optimum solid concentration was also observed in earlier pipe reactor experiments. In terms of absolute size comparison, Magnafloc produced larger aggregates than Rheomax at a solid concentration of 5% w/w; approximately equal at 10% w/w; and smaller for 15 and 20% w/w. An increase in the inlet velocity did reduce the mean aggregate size for all cases but did not alter the general trends.

The increased aggregate density for flocculation with Rheomax also resulted in higher settling velocities than compared to Magnafloc. Even at the lowest solid concentration, the trade-off between size and density resulted in the Rheomax having a higher settling velocity despite of having a significantly smaller size.

Combining the solid volume fraction and settling velocity, a theoretical limit on the solid extraction throughput was estimated. Results showed that Rheomax outperformed the Magnafloc for all cases in terms of this metric. Since the present study did not incorporate modelling of the compressive and shear rheology of the sediment, further work will be required to ascertain its impact on thickener performance.

ACKNOWLEDGEMENT

This work was conducted as a collaborative project between CSIRO and BASF. It utilised modelling techniques developed by CSIRO through the AMIRA P266 'Improving Thickener Technology' series of projects, of which BASF is a sponsor.

REFERENCES

ADKINS S.J., (2008), "Underflow rheology optimisation to enhance thickener performance", *Paste 2008: Proceedings of the Eleventh International Seminar on Paste and Thickened Tailings*, Australian Centre for Geomechanics, Perth, Australia, 83-95.

BATTERHAM R.J., HALL J.S. and BARTON G., (1981), "Pelletizing kinetics and simulation of full-scale balling circuits", *Proc. 3rd Int. Symp. on Agglomeration*, Nurnberg, W. Germany, A136.

BERKOWITZ B., NAUMANN C. and SMITH L., (1994), "Mass transfer at fracture intersections: an evaluation of mixing models", *Water Resour. Res.*, **30**, 1765-1773.

GOVIER C.W. and AZIZ K., (1972), "The flow of complex mixtures in pipes", *Melbourne: Van Nostrand Reinhold Company*.

GRABSCH A.F., FAWELL P.D., ADKINS S.J. and BEVERIDGE A., (2012), "How achieving a higher aggregate density through flocculant selection can impact upon polymer-bridging flocculation", Submitted to *Inter. J. Min. Process.*

HEATH A.R., BAHRI P.A., FAWELL P.D. and FARROW J.B. (2006), "Polymer flocculation of calcite: population balance model", *AICHE Journal*, **52**, 1641-1653.

HEATH A.R., KOH P.T.L. (2003), "Combined population balance and CFD modelling of particle aggregation by polymeric flocculant", *Third International Conference on CFD in the Mineral and Process Industries*. CSIRO, Melbourne, Australia, 339-344.

HOUNSLOW M.J., RYALL R.L. and MARSHALL V.R., (1988), "A discretised population balance for nucleation, growth and aggregation", *AICHE Journal*, **34**, 1821-1832.

HULL L.C. and KOSLOW K.N., (1986), "Streamline routing through fracture junctions", *Water Resour. Res.*, **22**, 1731-1734.

NGUYEN T., FARROW J.B., SMITH J. and FAWELL P.D., (2012), "Design and development of a novel thickener feedwell using computational fluid dynamics", *Paste 2012: Proceedings of the Fifteenth International Seminar on Paste and Thickened Tailings*, Australian Centre for Geomechanics, Sun City, South Africa, 105-120.

NGUYEN T., HEATH A. and WITT P., (2006), "Population balance - CFD modelling of fluid flow, solids distribution and flocculation in thickener feedwells", *Fifth International Conference on CFD in the Process Industries*, CSIRO, Melbourne, Australia, 13-15 December 2006.

POTANIN A.A. and URIEV N.B., (1991), "Microrheological models of aggregated suspensions in shear flow", *Journal of Colloid and Interface Science*, **142**, 385-395.

RICHARDSON J.F. and ZAKI W.N., (1955), "Sedimentation and fluidisation", *Trans. Instn. Chem. Engrs.*. **32**, 35-53.

RODES M.E. and BLUNT M.J., (2006), "An exact particle tracking algorithm for advective-dispersive transport in networks with complete mixing at nodes", *Water Resour. Res.*, **42**, W04501.

SMITH L. and SCHWARTZ F.W., (1983), "A stochastic analysis of macroscopic dispersion in fractured media", *Water Resour. Res.*, **19**, 1253-1265.

SMITH L. and SCHWARTZ F.W., (1984), "An analysis of the influence of fracture geometry on mass transport in fractured media", *Water Resour. Res.*, **20**, 1241-1252.

